Effect of Standing Wave on Terahertz Channel Model

Ha Tran
Department of ECE
Portland State University
Portland, OR 97207
Email: tranha@pdx.edu

Thanh Le
Department of ECE
Portland State University
Portland, OR 97207
Email: thanh4@pdx.edu

Suresh Singh
Department of Computer Science
Portland State University
Portland, OR 97207
Email: singh@cs.pdx.edu

Abstract—There is a growing interest in exploiting the terahertz frequency band for future communication systems that demand high data rates. Given the complex propagation behavior of this frequency band, various researchers have developed channel models that can be utilized in the development of communication systems. These models however do not include a crucial aspect of terahertz propagation at short distances – the presence of standing waves. Our measurements show that at specific distances, the effect of standing waves is significant. In this paper, we extend previous terahertz channel models to include the effect of standing waves and show a good fit with our measurements. Our measurements and modeling cover the five most promising terahertz frequency bands – 140, 220, 340, 410, 460 GHz.

Index Terms—Terahertz, channel model, line of sight.

I. INTRODUCTION

It is expected that wireless data needs will increase by three orders of magnitude over the next decade [1], leading to an intense interest in exploiting the largely unused terahertz band for future wireless needs. As [2] notes, terahertz frequencies can be deployed to support new massively broadband IoT for sensing and communications as well as enable the deployment of wireless fiber links to rural communities. However, this frequency band has several challenges including poor propagation, environmental impairments and a lack of devices that can work across ultra-wide bandwidths. As a result, there are several efforts underway aimed at examining different aspects of this frequency band with the goal of providing high data-rate communication channels.

One set of research approaches has focused on demonstrating high speed communication at specific sub-bands while another approach has combined channel measurements with modeling to predict the achievable data rates. For example, data rates of tens of gigabit per second (Gbps) for line of sight (LoS) and of several Gbps for non line of sight (NLoS) has been demonstrated at the 300-350 GHz frequency band [3]. Hirata et al [4] demonstrated 10 Gbps transmission at 120 GHz frequency over a distance of almost 6 km. Kallfass et al [5] demonstrated transmissions using OOK at 220 GHz and achieved 50 Gbps over 50 cm distances. Song et al [6] showed transmissions of 8 Gbps using ASK modulation over 250 GHz.

Most recently, Jia et al [7] demonstrated 106 Gbps at 400 GHz using a photonic wireless link. There have been many other demonstrations as well [8]–[13] though a notable one was by Koenig et al [14] in which they achieved 100 Gbps over 20 m using a phased antenna array.

Other works on examining the achievable data rates rely on channel measurement and modeling approaches. Using this method, [15] shows data rates of 1 Gbps are obtainable using 1 GHz wide frequency bands at 100, 200, 300, and 400 GHz. [16] shows that data rates of several Tbps (terabit/sec) are achievable utilizing acousto-optic modulation (AOM) over the entire frequency band in conjunction with careful rate adaptation algorithms.

A consequence of this flurry of work on terahertz over the past decade has been a better understanding of how these signals propagate in indoor and outdoor environments. One of the key observations [2] is that terahertz propagation differs significantly from millimeter wave in important ways including, higher phase noise and Doppler, significant diffraction effects as frequencies increase [17], and the presence of multiple arriving paths even without scatterers between the transmitter and receiver due to reflections from objects behind the transmitter and receiver. Furthermore, given the need for high-directivity antennas, we see somewhat different scattering patterns at terahertz as compared to millimeter wave [18].

Over the past year, we have been conducting measurements of a LoS channel using high directivity horn antennas [19], [20] at 140, 220, 340, 410, 460 GHz. These frequencies are identified as good Terahertz communication windows above 100GHz [21]. In addition to the effects observed by others, we noted a significant impact of a *standing wave* that gets established between the transmitter and receiver antennas. The effect of this is that the total attenuation at some distances is lower than we would expect if using a strict distance based attenuation as is typically done. *In this paper, we incorporate a model for the standing wave and develop an accurate channel model that correctly predicts the received signal for line of sight indoor channels.*

The remainder of the paper is organized as follows. In the next section, we present a brief overview of the current state of the art in terahertz channel models. Section III presents our channel model which is then compared against measurements

in section V. In section IV we describe our measurement setup as well as the experimental design for the channel measurements. We conclude in section VI.

II. Related Work

There has been considerable work on channel modeling for millimeter wave [1] and much of it is applicable to terahertz, with some modifications. Specific factors that need to be accounted for include frequency-dependent absorption due to water and other molecules, absence of many reflected paths due to material attenuation, consideration of high-gain antennas in propagation path estimation, frequency-dependent diffraction effects, presence of reflections between objects behind the transmitter and receiver (such as the body of the instrumentation), and, as we discovered, presence of *standing waves* at some distances.

One popular approach for building terahertz channel models is to utilize a Geometry-based Stochastic Channel Model (GSCM). In these models, ray-tracing is combined with geometrical properties of wave scattering objects modeled as random variables and an optics-based approach to model diffraction. Early ray-tracing path loss models for terahertz [22], [23] were enhanced by combining frequency-dependent path gain [24] with statistical models for multipath propagation [25] giving us a much improved model [26]. The first GSCM model for terahertz was proposed in [17], [18] for fixed point-to-point desktop communications. The model includes reflections that occur from behind the transmitter and receiver producing multiple paths to the receiver. [27] models frequency-based diffraction effects.

In our previous work [16] we constructed and validated a LoS channel model that added a frequency-based absorption coefficient to the standard Friis equation. Measurements with a time-domain system showed good agreement. However, the system uses HDPE lenses for creating collimating beams and as a result effects of diffraction, reflections, and other impairments are absent. In subsequent studies, we used a frequency-domain system and horn antennas to conduct measurements [19], [20] for modeling MIMO channels. We observed that as distance increased, at some points the attenuation did not change. Investigation revealed the presence of standing waves that appear to have a significant impact on the channel. We investigate this behavior below.

III. Channel Model

Our channel model is a modification of the *single-frequency floating intercept model* [28]. In this model, the path loss (PL) is written as,

$$\text{PL}(d) = \alpha + 10\beta \log_{10}\left(\frac{d}{d_0}\right) + X_\sigma, \ d \geq d_0 \qquad (1)$$

where d is the distance, $d_0 = 10$ cm is the reference distance, α is a floating intercept in dB that denotes the free-space path loss at d_0. The distance-based path loss exponent is β and X_σ is the large-scale shadow fading that is modeled as a zero-mean Gaussian with standard deviation σ. To estimate the parameters

α, β, σ we use a least squares linear fit such that the root mean square deviation from the mean path loss is minimized.

In our measurements, we observed that the attenuation remains almost constant for some distances before increasing again. We realized that this behavior occurs because standing waves created between the transmit and receive horn antennas increase the received signal strength. We therefore add an additional term to the above equation to account for this.

A. Standing Wave Model

We can write the received voltage due to the standing wave $V(d)$ at distance d as consisting of two components – the forward wave and the reflected wave [29]:

$$\begin{aligned} V_f(d) &= e^{-ik(d-d_0)}A \\ V_r(d) &= \Gamma e^{ik(d-d_0)}A \end{aligned} \qquad (2)$$

for some complex amplitude A (corresponding to the forward wave at d_0), k is the wavenumber, and Γ is the reflection coefficient. The superposition of these two waves gives,

$$\begin{aligned} V_{net}(d) &= V_f(d) + V_r(d) \\ &= e^{-ik(d-d_0)}(1 + \Gamma e^{i2k(d-d_0)})A \end{aligned} \qquad (3)$$

Therefore, the magnitude of the standing wave can be written as,

$$\begin{aligned} |V_{net}(d)|^2 &= V_{net}(d)V_{net}^*(d) \\ &= e^{-ik(d-d_0)}(1 + \Gamma e^{i2k(d-d_0)})A \\ &\quad e^{ik(d-d_0)}(1 + \Gamma^* e^{-i2k(d-d_0)})A^* \\ &= \left[1 + |\Gamma|^2 + 2\Re(\Gamma e^{i2k(d-d_0)})\right]|A|^2 \end{aligned} \qquad (4)$$

Since this quantity is added to the signal at the receiver, we need to subtract it (in dB) from the path loss formula in equation 1 to obtain the final model for path loss.
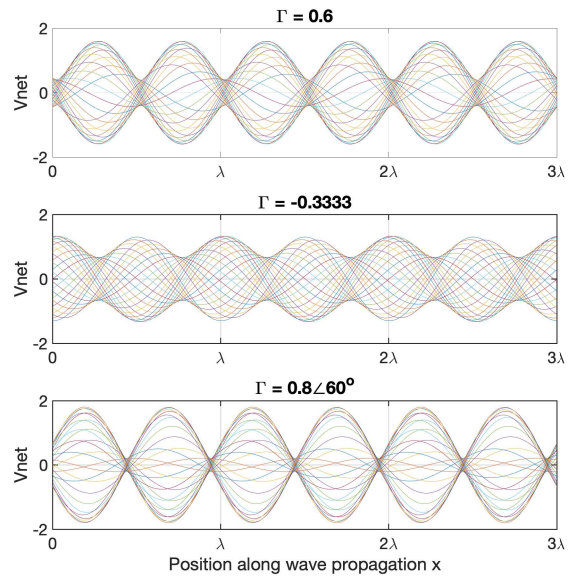
Fig. 1. Standing wave between the transmit and receive antennas.

In Figure 1 we plot the standing wave as a function of distance in term of λ for three different values of the reflection

coefficient Γ = 0.6, -0.333, 0.8∠60°. The standing wave ratio (SWR) coefficient V_{max}/V_{min} is 4, 2, 9 respectively. In Figure 2 we plot the amplitude of the standing wave for the three Γ values for different distances starting with d that is a multiple of $\lambda/2$ and then subsequent values reducing the distance by $\lambda/10$. From Figures 1 and 2, we can clearly see the effect of the standing wave on the received signal. Depending on the values of the complex reflection coefficient (its magnitude and phase), the magnitude of the standing wave can vary which leads to changes in the received signal.
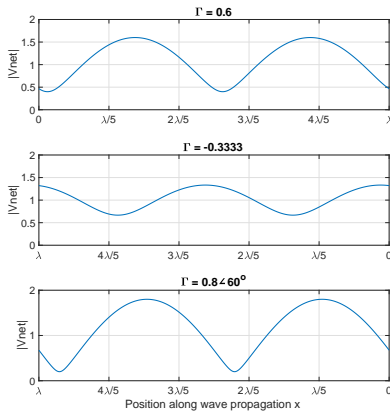
Fig. 2. Standing wave amplitude

IV. MEASUREMENT SETUP AND EXPERIMENTAL DESIGN
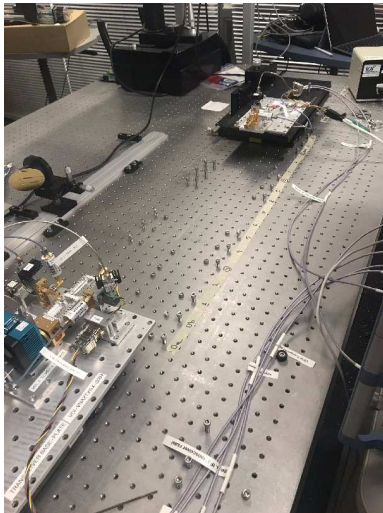
Fig. 3. Measurement setup.

We use a Rohde & Schwartz Vector Network Analyzer (VNA) and Virginia Diodes, Inc. (VDI) frequency extender system to conduct the measurements. The system is capable of producing signals up to 700 GHz. Figure 3 illustrates the setup for frequency band WR-6.5 (110-170 GHz). For this band, the transmit and receive antennas we use are horn antennas with gain of 21 dB and a 13^0 half power beam width (HBW). Measurements were conducted in the lab where the ambient

temperature was 72F and relative humidity was 40%. Other parameters of the experiment are given in Table I.

Notice that the horn antenna used for different frequency bands is different which also yields different received signals. The specifications of the VDI antennas for the measurements are given in Table II. Figure 4(a) demonstrates the 3D antenna pattern for WR-6.5 and the simulated antenna gain for investing frequencies are plotted in Figure 4(b).

V. MEASUREMENTS AND VALIDATION

To explain the process of fitting our model to the measured data, let us initially focus on measurements conducted at 140 GHz for varying distances. In Figure 5 we plot the measured data points and the *root mean square* (rms) fit for equation 1 to the data. While the trend of the fit is in good agreement, we observe that the actual data shows a curious behavior. We can see that for pairs of distances, the attenuation is flat. This happens due to the effects of the standing wave which gets established between the transmitter and receiver. In the next subsection, we explain how the fit is improved by incorporating equation 4 into the overall model. Subsequently, in section V-B, we show the model fit for the other frequencies.

A. Parameter Fitting

Equation 1 and 4 contain several parameters including α, β, Γ, k that we need to estimate from the measurements. Using the rms fit shown in Figure 5 we obtain α, β (shown in the figure). To find the reflection coefficient Γ and wavenumber k, we begin with the SWR,

$$\text{SWR} = \frac{V_{max}}{V_{min}} = \frac{1 + |\Gamma|}{1 - |\Gamma|}$$

which gives us,

$$|\Gamma| = \frac{V_{max} - V_{min}}{V_{max} + V_{min}}$$

In order to measure V_{max} and V_{min}, we utilize Figure 6 which is obtained by subtracting the fit in Figure 5 from the shown measured data points. We observe maximum and

(a) 3D antenna pattern for WR 6.5.
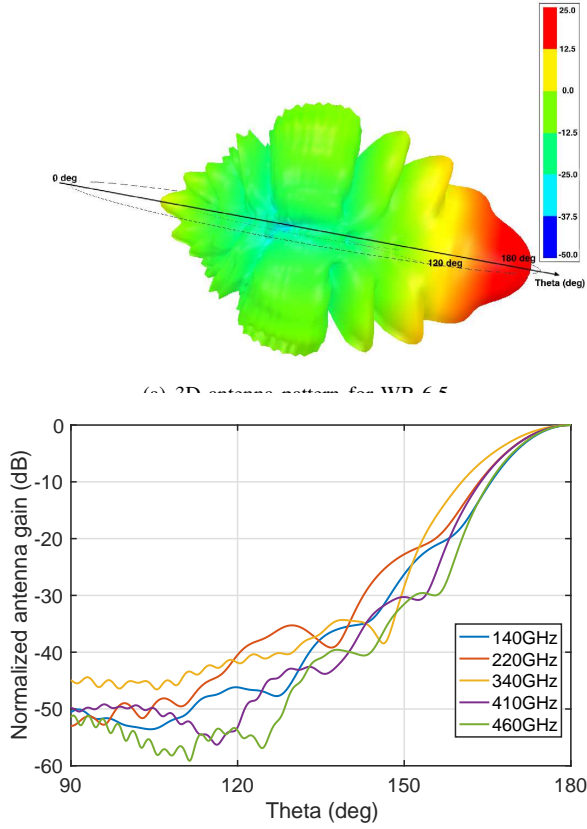
(b) Angular antenna gain for different frequencies.

Fig. 4. HFSS simulator output for antenna gain.
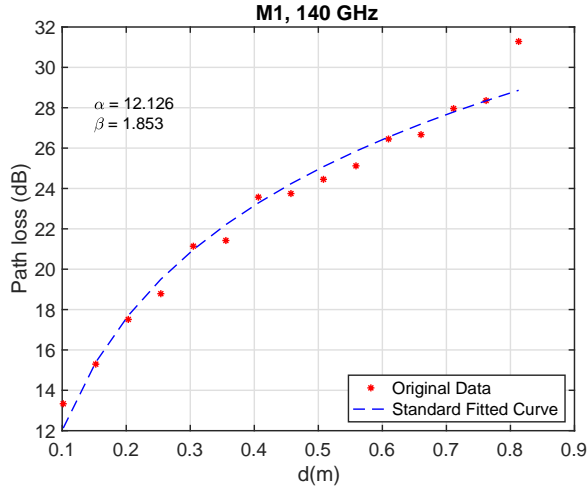
Fig. 5. Equation 1 rms fit to measured data for 140 GHz.

Fig. 6. Difference of fit and measured for 140 GHz.
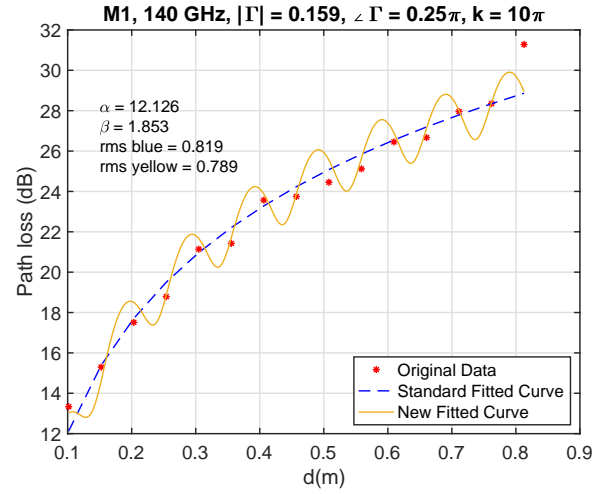
Fig. 7. Result of manual fit for Γ, k for 140 GHz.

minimum amplitudes (pointed out in the diagram). We utilize the largest and smallest values to the two maximum and minimum voltage levels. In our case, these values are 0.28 and -0.79 dB respectively. Using these values, we obtain $|\Gamma| = 0.158913332$ and the phase of Γ is 0.25π. The last parameter we need to estimate is the wavenumber k.

In equation 4 consider the term $\Re(\Gamma e^{i2k(d-d_0)})$. This is the real part of the complex term and can be represented as a cosine function of form $\cos(2k\pi d)$. By determining the distance between two consecutive maxima or minima in Figure 6, we obtain the period of the cosine, from which we can then directly read off the value of k. In Figure 6, this distance is 0.1m which gives an estimate of $k = 10\pi$ for 140 GHz. Using these values for Γ and k we plot the overall fit in Figure 7.

While this approach makes sense, there is one caveat – since we only have a few measurements, we might have missed the correct values for V_{max} and V_{min} as well as the correct k. Therefore, we finally conduct a fine tuning step where we begin with the manually obtained values and do a rms fit varying $|\Gamma|, k$ and the phase of Γ. This fit gives us Figure 8 where we see an improved agreement with the measured data. The figure also shows the rms values for equation 1 by itself and for our model which combines equation 1 with 4.

B. Model Fit for Different Frequencies

We utilize the methodology outlined above to fit the measured data for the other four frequency bands. **To make sure that there is no significant reflection from the metallic**
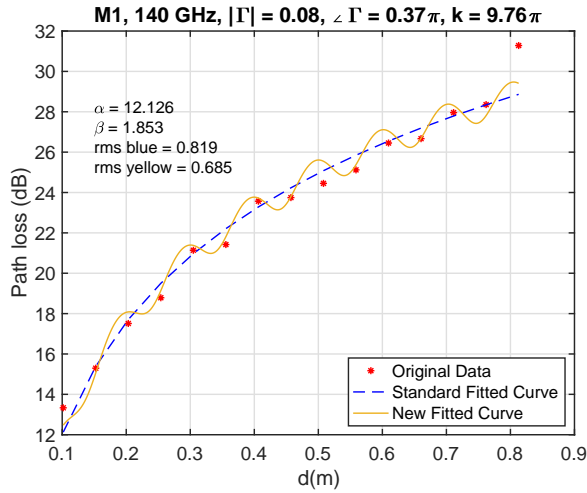
Fig. 8. Result of rms fit for Γ, k for 140 GHz.
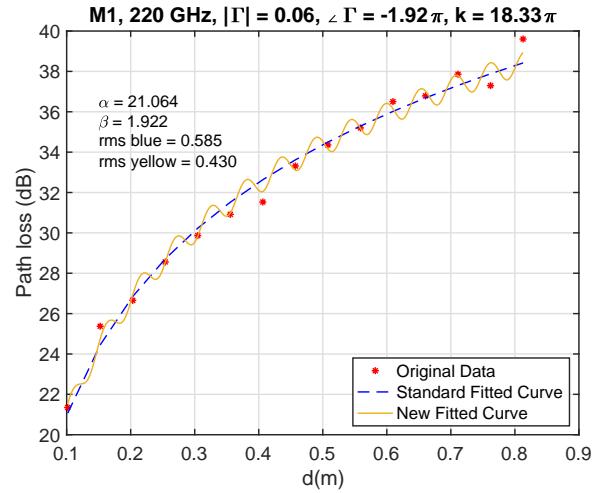
Fig. 10. Fit for 220 GHz.
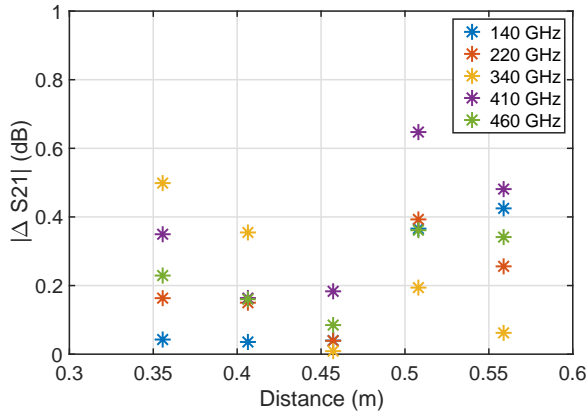
Fig. 9. Difference in received signal between with and without wet towel
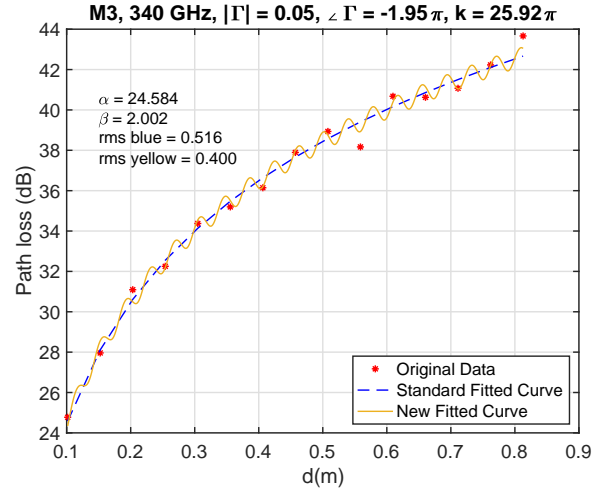
Fig. 11. Fit for 340 GHz.

surface of the measuring table, we compare the received signal in two cases: with and without a presence of a wet towel on top of the table which would absorb all reflections. Figure 9 shows that there is less than 0.5 dB difference in the signal between the two cases. Therefore, we conclude that the effect of reflections off the table is minimal.

In every frequency, we observe that the *rms* error is smaller for the model that includes the standing wave equation. The values of the antenna reflection coefficient magnitude for 140, 220, 340, 410, 460 GHz are 0.08, 0.06, 0.05, 0.09, 0.0988 respectively. We can see that with an exception of 140 GHz data, as frequency gets higher, more energy is reflected back by the antenna. This implies a need for careful antenna selection when designing terahertz systems. It is also interesting to see that the value of β in equation 1 is 1.85 - 2.04 for the different frequency bands, giving us a simple propagation model (i.e., no reflected components with the exception of the standing wave).

VI. CONCLUSION

In this paper, we examine the propagation behavior of five terahertz frequency bands, 140, 220, 340, 410, 460 GHz, when

using horn antennas at the transmitter and receiver. We modify existing channel models to include the effects of standing waves between the transmit and receive antennas. We show that at specific distances, these standing waves more than make up for the distance based attenuation. In other words, for certain distances and frequencies, as the distance increases, the attenuation falls. Our channel model provides an accurate fit for this behavior. For our future work, we will perform more measurements at finer distance granularity and examine other antenna types as well. We will also perform measurements in more complex propagation environments where there may be multiple reflectors in the path.

REFERENCES

[1] I. A. Hemadeh, K. Satyanarayana, M. El-Hajjar, and L. Hanzo. Millimeter-wave communications: Physical channel models, design considerations, antenna constructions, and link budgets. *IEEE Communications Surveys & Tutorials*, 20(2):870 – 913, 2018.
[2] Y. Xing, O. Kanhere, S. Ju, and T. S. Rappaport. Indoor wireless channel properties at millimeter wave and sub-terahertz frequencies. In *Proceedings IEEE GLOBECOM 2019*, pages 1 – 6, December 2019.
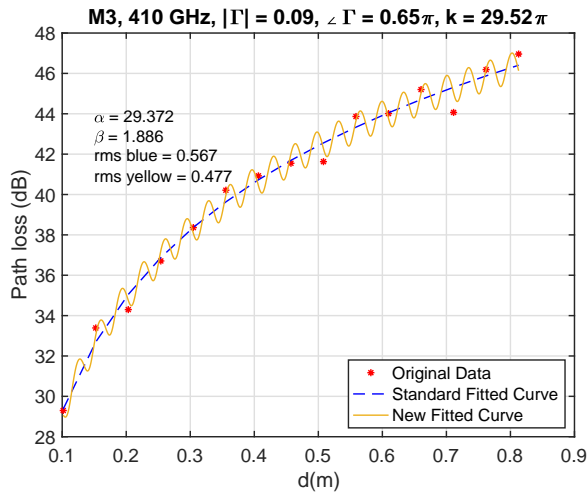
Fig. 12. Fit for 410 GHz.
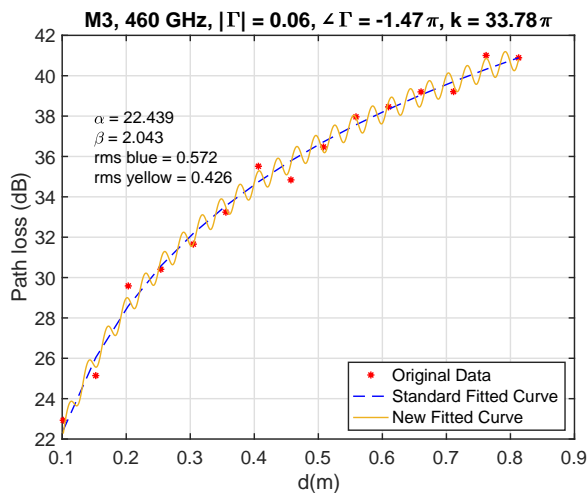
Fig. 13. Fit for 460 GHz.

[3] T. Kleine-Ostmann et al. Measurement of channel and propagation properties at 300ghz. In *Conference on precision electromagnetic measurements*, pages 258–259, July 2012.

[4] A. Hirata, T. Kosugi, H. Takahashi, J. Takeuchi, K. Murata, N Kukutsu, Y. Kado, S. Okabe, T. Ikeda, F. Suginosita, et al. 5.8-km 10-Gbps data transmission over a 120-GHz-band wireless link. In *2010 IEEE International Conference on Wireless Information Technology and Systems (ICWITS)*, pages 1–4. IEEE, 2010.

[5] Ingmar Kallfass, Jochen Antes, Thomas Schneider, Fabian Kurz, Daniel Lopez-Diaz, Sebastian Diebold, Hermann Massler, Arnulf Leuther, and Axel Tessmann. All active MMIC-based wireless communication at 220 GHz. *IEEE Transactions on Terahertz Science and Technology*, 1(2):477–487, November 2011.

[6] H.J. Song, K. Ajito, A. Hirata, A. Wakatsuki, T. Furuta, N. Kukutsu, and T. Nagatsuma. Multi-gigabit wireless data transmission at over 200-GHz. In *34th International Conference on Infrared, Millimeter, and Terahertz Waves, 2009. IRMMW-THz 2009*, pages 1–2, 2009.

[7] S. Jia, X. Pang, O. Ozolins, X. Yu, H. Hu, J. Yu, P. Guan, F. Da Ros, S. Popov, G. Jacobsen, M. Galili, T. Morioka, D. Zibar, and L. K. Oxenlowe. 0.4 thz photonic-wireless link with 106 gb/s single channel bitrate. *Journal of Lightwave Technology*, 36(2):610–616, January 2018.

[8] J. Antes, J. Reichart, D. Lopez-Diaz, A Tessmann, F. Poprawa, F. Kurz, T. Schneider, H. Massler, and I. Kallfass. System concept and implementation of a mmW wireless link providing data rates up to 25 Gbit/s. In *2011 IEEE International Conference on Microwaves, Communications,*

Antennas and Electronics Systems (COMCAS), pages 1–4, Nov 2011.

[9] Bo Zhang, Yong-Zhong Xiong, Lei Wang, and Sanming Hu. A switch-based ASK modulator for 10 Gbps 135 GHz communication by 0.13 MOSFET. *IEEE Microwave and Wireless Components Letters*, 22(8):415–417, 2012.

[10] H.J. Song, K. Ajito, Y. Muramoto, and A. Wakatasuki. 24 Gbit/s data transmission in 300 GHz band for future terahertz communications. *Electronics Letters*, 48(15):953–954, July 2012.

[11] Guillaume Ducournau, Pascal Szriftgiser, Alexandre Beck, Denis Bacquet, Fabio Pavanello, Emilien Peytavit, Mohammed Zaknoune, Tahsin Akalin, and J-F Lampin. Ultrawide-bandwidth single-channel 0.4-THz wireless link combining broadband quasi-optic photomixer and coherent detection. 2014.

[12] Cheng Wang, Changxing Lin, Qi Chen, Bin Lu, Xianjin Deng, and Jian Zhang. A 10-Gbit/s wireless communication link using 16-QAM modulation in 140-GHz band. *IEEE Transactions on Microwave Theory and Techniques*, 61(7):2737–2746, July 2013.

[13] Bin Lu, Wei Huang, C Lin, and C Wang. A 16QAM modulation based 3Gbps wireless communication demonstration system at 0.34 THz band. In *Infrared, Millimeter, and Terahertz Waves (IRMMW-THz), 2013 38th International Conference on*, pages 1–2. IEEE, 2013.

[14] S. Koenig, D. Lopez-Diaz, J. Antes, F. Boes, R. Henneberger, A. Leuther, A. Tessmann, R. Schmogrow, D. Hillerkuss, R. Palmer, T. Zwick, C. Koos, W. Freude, O. Ambacher, J. Leuthold, and I. Kallfass. Wireless sub-THz communication system with high data rate. *Nature Photonics*, 7:977–981, October 2013.

[15] J. Ma, R. Shrestha, L. Moeller, and D. M. Mittleman. Channel performance for indoor and outdoor terahertz links. 3(5):1–13, Feb. 2018.

[16] F. Moshir and S. Singh. Modulation and rate adaptation algorithms for terahertz channels. September 2016.

[17] S. Kim and A. Zajic. Statistical modeling of the thz scatter channels. In *Proceedings IEEE European Conference on Antennas and Propagation EuCAP15*, pages 1–5, April 2015.

[18] S. Kim and A. Zajic. Statistical modeling and simulation of short-range device-to-device communications channel at sub-thz frequencies. pages 6423–6433, September 2016.

[19] S. Singh, H. Tran, and T. Le. Challenges in los terahertz mimo. In *Proceedings IEEE GLOBECOM*, Hawaii, December 2019.

[20] S. Singh, T. Le, and H. Tran. Measurement of 2x2 los terahertz mimo channel'. In *Proceedings IEEE WCNC*, Seoul, S. Korea, April 2020.

[21] John Federici and Lothat Moeller. Review of terahertz and subterahertz wireless communications. *Journal of Applied Physics*, 107, 2010.

[22] C. Jansen et al. The impact of reflections from stratified building materials on the wave propagation in future indoor terahertz communication systems. *IEEE Transactions on Antennas and Propagation*, 56(5):1413 – 1419, May 2008.

[23] S. Priebe, M. Jacob, C. Jastrow, T. Kleine-Ostermann, T. Schrader, and T. Kurner. A comparison of indoor channel measurements and ray tracing simulations at 300 ghz. In *Proceedings International Conference on Infrared Millimeter and Terahertz Waves (IRMMW-THz)*, 2010.

[24] A. F. Molisch. Ultrawideband propagation channels-theory, measurement, and modeling. 54(5):1528–1545, September 2005.

[25] A. Saleh and R. Valenzuela. A statistical model for indoor multipath propagation. *IEEE Journal on Selected Areas in Communications*, 5(2):128 – 137, May 1987.

[26] S. Priebe and T. Kurner. Stochastic modeling of thz indoor radio channels. *IEEE Transactions on Wireless Communications*, 12(9):4445 – 4455, September 2013.

[27] C. Han, A. O. Bicen, and I. F. Akyilidiz. Multi-ray channel modeling and wideband characterization for wireless communications in the thz band. *IEEE Transactions on Wireless Communications*, 14(5):2402 – 2412, May 2015.

[28] C.-L. Cheng, S. Kim, and A. Zajic. Comparison of path loss models for indoor 30 ghz, 140 ghz, and 300 ghz channels. In *Proceedings 11th European Conference on Antennas and Propagation (EUCAP)*, pages 716–720, Paris, france, March 2017.

[29] David M. Pozar. *Microwave Engineering*. Wiley, 4th edition, 2011.